nature photonics

LETTERS

https://doi.org/10.1038/s41566-021-00778-y

Check for updates

A six-octave optical frequency comb from a scalable few-cycle erbium fibre laser

Daniel M. B. Lesko[1,2,4] ✉, Henry Timmers[1,4], Sida Xing[1,3], Abijith Kowligy[1,3], Alexander J. Lind[1,3] and Scott A. Diddams[1,3] ✉

A coherent, compact and robust light source with coverage from the ultraviolet to the infrared is desirable for heterodyne super-resolution imaging[1], broadband infrared microscopy[2], protein structure determination[3] and standoff trace-gas detection[4]. To address these demanding problems, frequency combs[5] combine absolute frequency accuracy with sub-femtosecond timing and waveform control to enable high-resolution, high-speed and broadband spectroscopy[6–9]. Here we demonstrate a scalable source of near-single-cycle pulses from robust and low-noise erbium fibre (Er:fibre) technology. With a peak power of 0.56 MW we generate a comb spanning six octaves, from the ultraviolet (350 nm) to the mid-infrared (22,500 nm), achieving a resolving power of 10^{10} across 0.86 PHz of bandwidth. Second-order nonlinearities in $LiNbO_3$, GaSe and $CdSiP_2$ provide phase-stable infrared ultrashort pulses with simultaneous brightness exceeding a synchrotron[10], while cascaded nonlinearities in $LiNbO_3$ yield four octaves simultaneously (0.350–5.6 μm). We anticipate that these advances will be enabling for basic and applied spectroscopy, microscopy and phase-sensitive nonlinear optics.

Optical spectroscopy from the ultraviolet (UV) to the mid-infrared (MIR) has proved to be a critical technique for determining a molecule's precise structure and function in a non-destructive manner[11]. Spectroscopy is generally accomplished using different light sources for each wavelength regime of interest. However, utilizing a single coherent source that can cover multiple absorption bands and spectroscopic regimes will enable correlated, high-fidelity measurements of simultaneous processes that are critical to many analytical science fields, from how water vibrates[12], to how greenhouse gases bond to pollutant particles[13] and how proteins are structured[14]. The direct generation of broadband coherent sources is challenging, and therefore nonlinear frequency conversion (that is, $\chi^{(3)}$ supercontinuum[15] and $\chi^{(2)}$ parametric[16] processes) has proved to be an indispensable technique for generating coherent light at otherwise inaccessible wavelengths. The molecular fingerprint region represents one important spectroscopic area in which the direct generation of a broadband MIR source remains an open problem. Typically, direct emission from MIR quantum cascade laser combs can provide simultaneous coverage over 1–2 THz (ref. [17]). To achieve broader bandwidths, a common alternative is to employ nonlinear frequency conversion to shift the spectra of near-infrared (NIR) lasers to the MIR fingerprint region[18–22]. Leveraged by the global telecommunications infrastructure, NIR Er:fibre technology in particular offers commercially available ultralow-noise mode-locked laser oscillators, versatile dispersion-engineered and nonlinear fibres, as well as an inexpensive, fibre-integrated off-the-shelf component catalogue. This technology has demonstrated reliability, robustness and utility for generating frequency combs in applications including optical clock comparisons[23], optical frequency division[24], quantum vacuum metrology[25] and high-resolution spectroscopy[6].

A particularly simple way of generating ultra-broadband infrared radiation is through intra-pulse difference frequency generation (IP-DFG), where a NIR ultrashort pulse (<10 fs) is focused into a $\chi^{(2)}$ nonlinear medium and undergoes nonlinear mixing and down-conversion[26–28]. This process takes advantage of the $\chi^{(2)}$ susceptibility of the medium as opposed to the much weaker $\chi^{(3)}$ nonlinearity. An IP-DFG comb has a simple and robust architecture (no delay stage for temporal overlap or cavity for enhancement) while generating MIR coherent radiation with a simultaneous bandwidth as large as ~50 THz (ref. [7]). Additionally, the down-converted light is an ultrashort pulse that is passively carrier-envelope stable and can be further used as a seed for phase-stable MIR optical parametric chirped-pulse amplification[29].

The challenge in generating an IP-DFG comb is twofold: (1) the requirement of a few-cycle driving pulse at a high repetition rate (≥100 MHz) and (2) the high average power needed for MIR comb generation. In previous work[27,30], we presented a few-cycle Er:fibre comb generated from a core-pumped Er:fibre amplifier. The few-cycle comb was then used as a driver for IP-DFG to generate MIR light anywhere from 3 to 27 μm. However, owing to the limited power scaling of the core-pumped Er:fibre we were limited to 0.25 mW of MIR comb light from the IP-DFG process. In this Letter, we instead show how to use a cladding-pumped erbium/ytterbium co-doped fibre amplifier[31] (EYDFA), which is not subject to the same power-scaling limitations as the core-pumped system, to produce more energetic pulses at 1,550 nm whilst maintaining sub-10-fs pulses. When our 0.56 MW peak power source is used to drive IP-DFG, we now generate 3.5 mW of MIR comb light. Additionally, with this high-power, near-single-cycle comb source, we perform ultra-broadband frequency conversion with a single pass through infrared-transparent $\chi^{(2)}$ nonlinear crystals to generate multi-octave combs spanning from the MIR to the UV. Our analysis further shows that the amplification and spectral broadening process is scalable from 1 to 100 nJ while maintaining 10 fs pulses, substantially expanding the application space of Er:fibre comb technology.

We describe our experiment in Fig. 1. The pulse first is amplified in a pre-amplifier and subsequently stretched with a dispersion-compensating fibre before it seeds a chirped-pulse EYDFA. The pre-amplifier limits the gain narrowing in the

[1]Time and Frequency Division, National Institute of Standards and Technology, Boulder, CO, USA. [2]Department of Chemistry, University of Colorado, Boulder, CO, USA. [3]Department of Physics, University of Colorado, Boulder, CO, USA. [4]These authors contributed equally: Daniel M. B. Lesko, Henry Timmers. ✉e-mail: Daniel.Lesko@nist.gov; Scott.Diddams@nist.gov

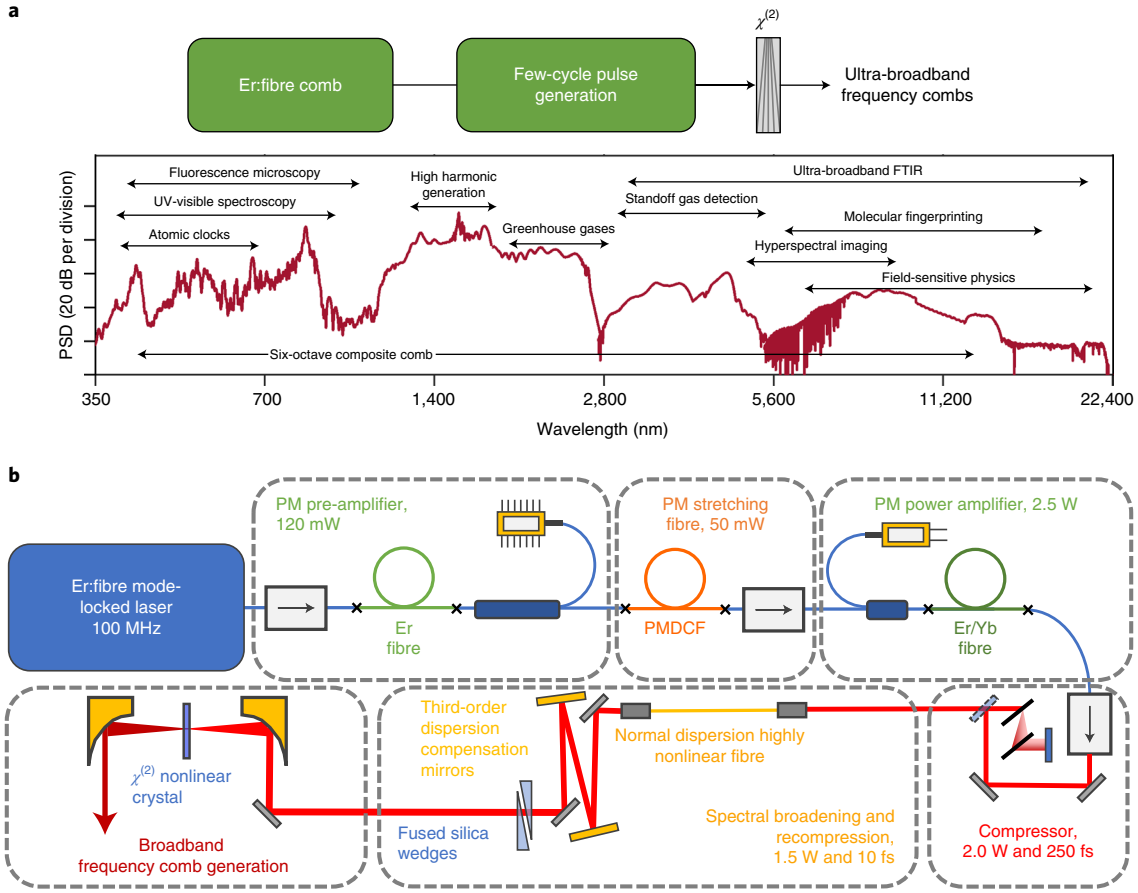

Fig. 1 | Generation and applications of a six-octave frequency comb. a, An Er:fibre mode-locked laser comb at 1,550 nm seeds the generation of a few-cycle pulse to drive frequency conversion in second-order ($\chi^{(2)}$) nonlinear crystals (above). The resulting composite spectrum (below), generated in three nonlinear crystals, spans six octaves for a wide range of applications, as shown. PSD, power spectral density. FTIR, Fourier transform infrared. **b**, Schematic of the fibre amplification and short pulse generation. PM, polarization-maintaining. See text for details.

second stage of amplification. The amplified pulse is subsequently compressed via a grating compressor to generate a 250 fs pump pulse with an average power of 2.5 W, for which the reconstructed second harmonic generation frequency-resolved optical gating (SHG-FROG) is shown in Fig. 2a. We then broaden the pump pulse in normal dispersion highly nonlinear fibre (ND-HNLF) to a bandwidth that supports a <10 fs pulse. Spectral broadening and compression to <10 fs has also been done with anomalous dispersion HNLF and prism compressors. However, in such a case the pulses are typically <1 nJ and the spectral centre is shifted from 1,550 nm (ref. [32]). By contrast, the normal dispersion broadening we employ can be scaled to higher energies, it minimizes noise and ensures a clean phase accumulation that can be recompressed with bulk fused silica. Here we employ bulk UV fused silica and a pair of third-order dispersion-compensating mirrors (Fig. 2b), resulting in a compressed 9.4 fs pulse of 0.56 MW peak power. The corresponding experimental and retrieved pulses (Fig. 2c,d) show good agreement (1.5% root mean square FROG error). Furthermore, a model employing the nonlinear Schrödinger equation (NLSE) yields good agreement with both the spectrum and temporal profile of our experimental measurements. Details are in the Supplementary Information. Furthermore, our use of commercial off-the-shelf components allows for replication and use in a variety of laboratories and environments.

In Fig. 2e, we illustrate the potential of our approach to scale the pulse energy while maintaining a 10 fs pulse. Here we model the spectral broadening of the ND-HNLF with a simple analytic solution (Supplementary Information equation (2)) and with the NLSE for several chirped-pulse amplifier regimes up to 60 nJ (ref. [31]). Each contour represents the length of HNLF required to support a 10 fs pulse as the pulse energy is increased. Full details of the simulations used to generate Fig. 2e, including the realistic prediction of the 10 fs pulses at energies from 10 nJ to 100 nJ, are given in the Supplementary Information. The divergence of the dashed line from the solid contour occurs at ND-HNLF lengths for which the role of dispersion becomes important. The use of non-PM ND-HNLF results in unequal amounts of self-phase modulation occurring along orthogonal axes (Fig. 2f) as well as a reduction in the polarization extinction ratio (from 13 to 6 dB). This results in a longer HNLF required for the same level of spectral broadening (73 mm from theory to 110 mm in experiment). However, this should be corrected with PM ND-HNLF.

Ultra-broadband $\chi^{(2)}$ frequency conversion is performed with this near-single-cycle pulse in three crystals to generate spectra that yield coverage over six octaves of bandwidth (Fig. 3). Periodically poled lithium niobate ($LiNbO_3$, PPLN) yields both 3.5 mW of MIR light (3–5 μm) as well as harmonic generation and dispersive wave generation via cascaded $\chi^{(2)}$ (350–850 nm and 1.75–2.7 μm respectively). See Methods for more details. To extend the wavelength further into the infrared, a 560-μm-thick cadmium silicon phosphide ($CdSiP_2$, CSP) crystal or 1-mm-thick gallium selenide (GaSe) are used to generate 3 and 1.6 mW respectively. Three times

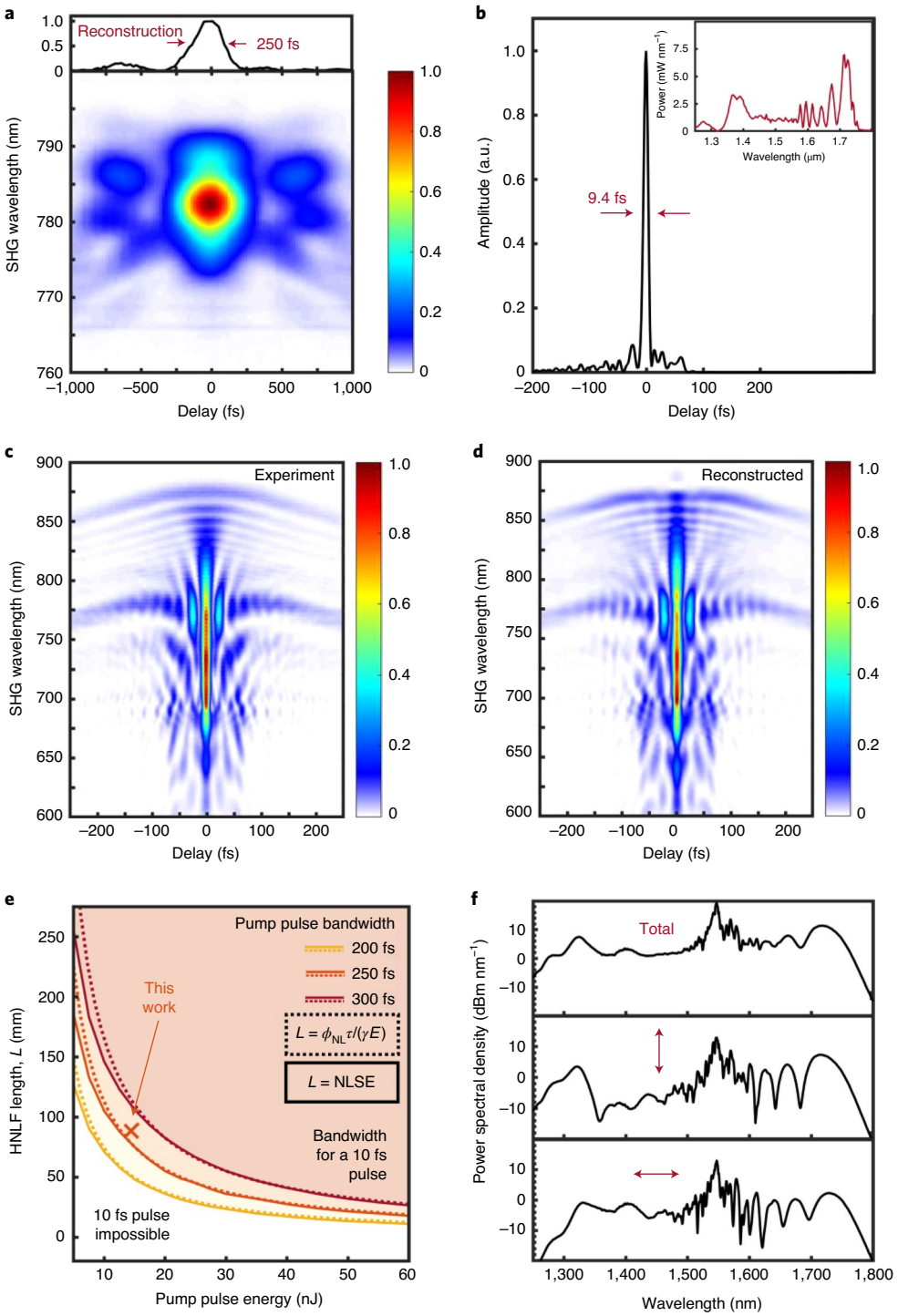

Fig. 2 | Data and simulations demonstrating scalable near-single-cycle pulse generation. a, SHG-FROG of the chirped-pulse amplifier output and the reconstructed 250 fs pulse. **b**, Retrieved temporal intensity profile of the 9.4 fs pulse and its spectrum (inset) that result from propagation in the ND-HNLF. **c**, Experimental SHG-FROG of the sub-two-cycle pulse. **d**, Reconstructed SHG-FROG of the sub-two-cycle pulse with a root mean square error of 1.5%. **e**, NLSE simulations (solid lines) and analytic solution (dashed lines) for scaling the HNLF length as a function of the pump pulse energy and full-width at half-maximum bandwidth. Each contour represents the fibre length needed to support 10 fs pulses, given the specified pump pulse. ϕ_{NL}, nonlinear phase; τ, temporal duration; γ, fibre nonlinearity; E, pump pulse energy. **f**, Polarization-dependent spectral broadening occurring in non-PM HNLF. The spectra measured in horizontal, vertical and both (total) polarizations are shown.

greater power could be achieved with anti-reflection coatings on the crystals.

We confirm that the resulting six-octave source is a coherent frequency comb at both extremes. At the high-frequency end, we observe the carrier envelope offset frequency (f_{ceo}) heterodyne beat at 445 nm, resulting from interference between the third and fourth harmonic ($3f$–$4f$ heterodyne); at the low-frequency end, we directly resolve individual comb teeth through dual-comb electro-optic

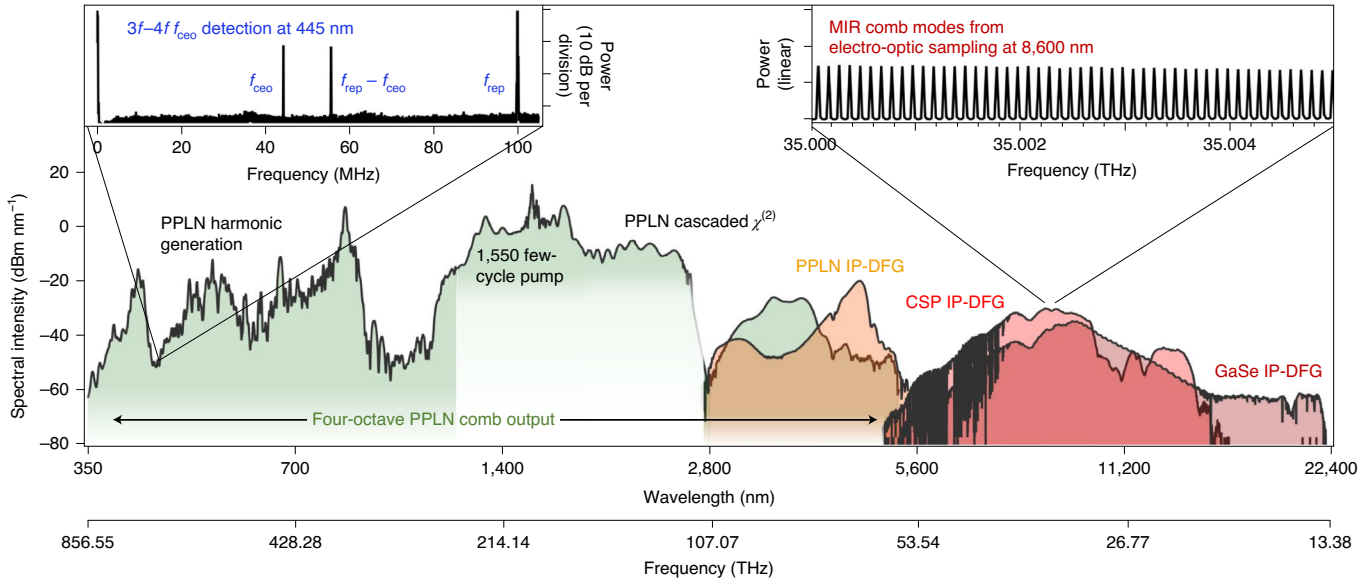

Fig. 3 | Six octaves of frequency comb coverage. Frequency conversion from the 1,550 nm, 0.56 MW few-cycle pump is achieved via $\chi^{(2)}$ nonlinearity in PPLN, CSP and GaSe crystals. The different colours represent spectra achieved under four unique sets of experimental conditions. One setting of the PPLN gives simultaneous coverage from 350 to 5,500 nm (shown in green), while a second configuration gives selective coverage in the MIR (orange). Similarly, single CSP and GaSe spectra are also shown (two shades of red). Here we present the broadest IP-DFG spectra obtained, but different coverage can be achieved by changing the poling periods or angle tuning the nonlinear crystals. The upper left inset shows f_{ceo} measurement at 445 nm from harmonic generation in PPLN. The upper right inset shows comb mode resolution of the infrared light from CSP measured with dual-comb electro-optic sampling.

sampling[7] with acquisition out to 22.4 µm. To switch between and optimize the spectral modes of the broadband comb, we tune or change nonlinear crystals and adjust the dispersion (fused silica wedges). See Methods.

In Fig. 4a, we compare the MIR output of our compact (~1 m^2) fibre-based coherent frequency comb with the Advanced Light Source at Lawrence Berkeley National Laboratory, for which we plot the maximum achievable infrared PSD under the operating conditions of 500 mA (ref. [10]). Our table-top experiment realizes the infrared spectrum of a synchrotron, providing a higher PSD over two simultaneous octaves of bandwidth than infrared synchrotron sources (Fig. 4a)[10,33]. These carrier envelope phase (CEP) stable pulses are few-cycle and transform-limited (measured by electro-optic sampling, Fig. 4b,d), and will be useful in subcycle quantum squeezing and quantum-sensing applications[34]. The residual phase measured in Fig. 4c,e arises from higher-order dispersion from a germanium beam splitter as well as atmospheric water contamination. This few-cycle and near-transform-limited infrared pulse, enabled by extremely broad phase matching and precise pump dispersion control, has not been achieved with other infrared comb systems[18,21,22,35].

In summary, we present a simple, robust and scalable architecture for generating megawatt-scale peak power few-cycle pulses with ultralow-noise Er:fibre comb technology. With these few-cycle pulses, we are able to generate a coherent 'light bulb', spanning six octaves (four simultaneously), utilizing only the second-order susceptibility of nonlinear crystals. We anticipate that this ultra-broadband coherent source will enable new modalities in hyperspectral imaging and nanoscopy, as well as opportunities to study chemical and biological processes over extreme spectral bandwidths and timescales.

Finally, these results provide a defined path for scaling the energy of sub-10-fs pulses produced with Er:fibre frequency comb technology to the 50 nJ regime, where peak intensities of >10 TW cm^{-2} will be accessible. This should enable new physical regimes to be explored with robust 1,550 nm fibre laser technology, including the direct generation of extreme UV frequency combs[36] and attosecond pulses in solids and gases[37] without the need for enhancement cavity geometries.

Online content

Any methods, additional references, Nature Research reporting summaries, source data, extended data, supplementary information, acknowledgements, peer review information; details of author contributions and competing interests; and statements of data and code availability are available at https://doi.org/10.1038/s41566-021-00778-y.

Received: 26 May 2020; Accepted: 6 February 2021;
Published online: 11 March 2021

References

1. Yang, F., Tashchilina, A., Moiseev, E. S., Simon, C. & Lvovsky, A. I. Far-field linear optical superresolution via heterodyne detection in a higher-order local oscillator mode. *Optica* **3**, 1148–1152 (2016).
2. Wetzel, D. L. & LeVine, S. M. Imaging molecular chemistry with infrared microscopy. *Science* **285**, 1224–1225 (1999).
3. Williams, R. W. & Dunker, A. K. Determination of the secondary structure of proteins from the amide I band of the laser Raman spectrum. *J. Mol. Biol.* **152**, 783–813 (1981).
4. Rieker, G. B. et al. Frequency-comb-based remote sensing of greenhouse gases over kilometer air paths. *Optica* **1**, 290–298 (2014).
5. Diddams, S. A., Vahala, K. & Udem, T. Optical frequency combs: coherently uniting the electromagnetic spectrum. *Science* **369**, eaay3676 (2020).
6. Coddington, I., Newbury, N. & Swann, W. Dual-comb spectroscopy. *Optica* **3**, 414–426 (2016).
7. Kowligy, A. S. et al. Infrared electric field sampled frequency comb spectroscopy. *Sci. Adv.* **5**, eaaw8794 (2019).
8. Ideguchi, T. et al. Coherent Raman spectro-imaging with laser frequency combs. *Nature* **502**, 355–358 (2013).
9. Bjork, B. J. et al. Direct frequency comb measurement of OD + CO → DOCO kinetics. *Science* **354**, 444–448 (2016).
10. Bosch, R. A. Computed flux and brightness of infrared edge and synchrotron radiation. *Nucl. Instrum. Methods Phys. Res. A* **454**, 497–505 (2000).
11. Hollas, J. M. *Modern Spectroscopy* 4th edn (Wiley, 2004).

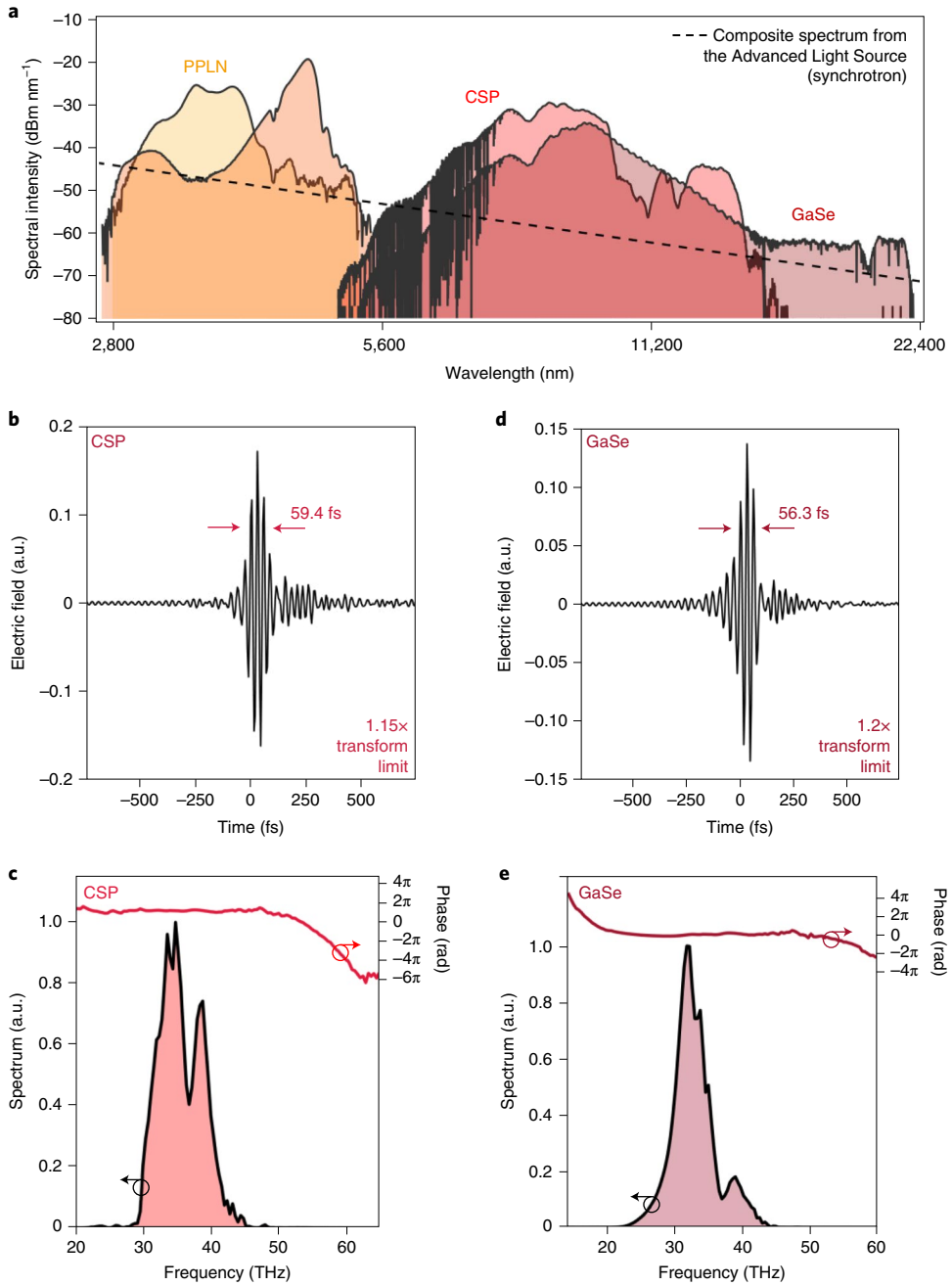

Fig. 4 | MIR few-cycle pulses and frequency combs. a, Comparison of MIR comb generation from IP-DFG with the composite spectrum calculated from the Advanced Light Source (~500 mA). **b**,**c**, Measured electric field from CSP (**b**) and the resulting spectrum and phase (**c**). **d**,**e**, Measured electric field from GaSe (**d**) and the resulting spectrum and phase (**e**).

12. Ramasesha, K., De Marco, L., Mandal, A. & Tokmakoff, A. Water vibrations have strongly mixed intra- and intermolecular character. *Nat. Chem.* **5**, 935–940 (2013).
13. Ostaszewski, C. J. et al. Effects of coadsorbed water on the heterogeneous photochemistry of nitrates adsorbed on TiO_2. *J. Phys. Chem. A* **122**, 6360–6371 (2018).
14. Mendelsohn, R., Flach, C. R. & Moore, D. J. Determination of molecular conformation and permeation in skin via IR spectroscopy, microscopy, and imaging. *Biochim. Biophys. Acta Biomembr.* **1758**, 923–933 (2006).
15. Dudley, J. M., Genty, G. & Coen, S. Supercontinuum generation in photonic crystal fiber. *Rev. Mod. Phys.* **78**, 1135–1184 (2006).
16. Vasilyev, S. et al. Multi-octave visible to long-wave IR femtosecond continuum generated in Cr:ZnS-GaSe tandem. *Opt. Express* **27**, 16405–16412 (2019).
17. Hugi, A., Villares, G., Blaser, S., Liu, H. C. & Faist, J. Mid-infrared frequency comb based on a quantum cascade laser. *Nature* **492**, 229–233 (2012).
18. Steinle, T., Mörz, F., Steinmann, A. & Giessen, H. Ultra-stable high average power femtosecond laser system tunable from 1.33 to 20 µm. *Opt. Lett.* **41**, 4863–4866 (2016).
19. Maidment, L., Schunemann, P. G. & Reid, D. T. Molecular fingerprint-region spectroscopy from 5 to 12 µm using an orientation-patterned gallium phosphide optical parametric oscillator. *Opt. Lett.* **41**, 4261–4264 (2016).
20. Gambetta, A. et al. Milliwatt-level frequency combs in the 8–14 µm range via difference frequency generation from an Er:fiber oscillator. *Opt. Lett.* **38**, 1155–1157 (2013).
21. Soboń, G., Martynkien, T., Mergo, P., Rutkowski, L. & Foltynowicz, A. High-power frequency comb source tunable from 2.7 to 4.2 µm based on difference frequency generation pumped by an Yb-doped fiber laser. *Opt. Lett.* **42**, 1748–1751 (2017).
22. Smolski, V. et al. Half-Watt average power femtosecond source spanning 3–8 µm based on subharmonic generation in GaAs. *Appl. Phys. B* **124**, 101 (2018).

23. Rosenband, T. et al. Frequency ratio of Al^+ and Hg^+ single-ion optical clocks; metrology at the 17th decimal place. *Science* **319**, 1808–1812 (2008).
24. Nakamura, T. et al. Coherent optical clock down-conversion for microwave frequencies with 10^{-18} instability. *Science* **368**, 889–892 (2020).
25. Riek, C. et al. Direct sampling of electric-field vacuum fluctuations. *Science* **350**, 420–423 (2015).
26. Huber, R., Brodschelm, A., Tauser, F. & Leitenstorfer, A. Generation and field-resolved detection of femtosecond electromagnetic pulses tunable up to 41 THz. *Appl. Phys. Lett.* **76**, 3191–3193 (2000).
27. Timmers, H. et al. Molecular fingerprinting with bright, broadband infrared frequency combs. *Optica* **5**, 727–732 (2018).
28. Pupeza, I. et al. High-power sub-two-cycle mid-infrared pulses at 100 MHz repetition rate. *Nat. Photon.* **9**, 721–724 (2015).
29. Elu, U. et al. High average power and single-cycle pulses from a mid-IR optical parametric chirped pulse amplifier. *Optica* **4**, 1024–1029 (2017).
30. Lind, A. J. et al. Mid-infrared frequency comb generation and spectroscopy with few-cycle pulses and $\chi^{(2)}$ nonlinear optics. *Phys. Rev. Lett.* **124**, 133904 (2020).
31. Elahi, P., Kalaycıoğlu, H., Li, H., Akçaalan, Ö. & Ilday, F. Ö. 175 fs-long pulses from a high-power single-mode Er-doped fiber laser at 1550 nm. *Opt. Commun.* **403**, 381–384 (2017).
32. Krauss, G. et al. Synthesis of a single cycle of light with compact erbium-doped fibre technology. *Nat. Photon.* **4**, 33–36 (2010).
33. Bechtel, H. A., Johnson, S. C., Khatib, O., Muller, E. A. & Raschke, M. B. Synchrotron infrared nano-spectroscopy and -imaging. *Surf. Sci. Rep.* **75**, 100493 (2020).
34. Riek, C. et al. Subcycle quantum electrodynamics. *Nature* **541**, 376–379 (2017).
35. Chaitanya Kumar, S. et al. High-power femtosecond mid-infrared optical parametric oscillator at 7 μm based on $CdSiP_2$. *Opt. Lett.* **40**, 1398–1401 (2015).
36. Jones, R. J., Moll, K. D., Thorpe, M. J. & Ye, J. Phase-coherent frequency combs in the vacuum ultraviolet via high-harmonic generation inside a femtosecond enhancement cavity. *Phys. Rev. Lett.* **94**, 193201 (2005).
37. Krausz, F. & Ivanov, M. Attosecond physics. *Rev. Mod. Phys.* **81**, 163–234 (2009).

Methods

Short pulse generation. A 100 MHz ultralow-noise fibre laser (Menlo Systems) was amplified to 120 mW in an erbium-doped fibre amplifier (980 nm pump, Liekki Er80-4/125-HD-PM) and then stretched in PM dispersion-compensation fibre (PMDCF, Thorlabs) and amplified to 2.5 W in an EYDFA (980 nm pump, Coractive CSF-EY-10/128-PM, similar in design to ref. [31]). The pulse was compressed via a grating pair and subsequently broadened in 11 cm of ND-HNLF (dispersion, $D=-1.0\,\mathrm{ps\,nm^{-1}\,km^{-1}}$, $D_{slope}=0.006\,\mathrm{ps\,nm^{-2}\,km^{-1}}$). Coupling into the HNLF was done with two mirrors and an aspheric lens; the coupling efficiency remained constant day to day after a brief warm-up period. The output from the ND-HNLF was collimated with a commercially available FC/APC fibre-coupled $f=7$ mm off-axis parabolic mirror (Thorlabs). The beam then passed through a pair of anti-reflection-coated fused silica wedges (apex angle 14°) along with one pair of bounces on chirped mirrors that compensate residual third-order dispersion (−750 fs^3, SHG-FROG Fig. 2c,d). An $f=50.8$ mm off-axis parabolic mirror was used to focus the few-cycle pulse into the $\chi^{(2)}$ nonlinear crystal. The same collimation, wedges and focusing optics were used for all three crystals, making interchanging them straightforward. One of the two fused silica wedges was placed on a translation stage to allow rapid adjustment of the dispersion of the few-cycle 1,550 nm pulse. The entire process of changing crystals and optimizing the output spectrum for a particular application required only a few minutes.

Spectral generation and measurement. A 2 mm fan-out PPLN (26–35 µm) was used to generate spectra from 350 to 5,000 nm. Longer poling periods yielded more targeted 3–5 µm light, while shorter periods allowed additional cascaded nonlinearities such as harmonic generation (covering 350–850 nm with 30 mW total) as well as cascaded $\chi^{(2)}$ broadening (1.75–2.7 µm).

A combination of optical spectrum analysers (OSAs; 350–1,200 nm, 700–1,700 nm and 1,200–2,400 nm) was used to measure the visible and NIR spectra. The 1.8–5.5 µm section was measured using a commercial FTIR spectrometer. The spectra from 5 to 22.4 µm were measured using dual-comb electro-optic sampling[7] to retrieve the electric field and spectrum. The 1.8–2.7 µm dispersive wave was measured on both the OSA and FTIR instruments, but owing to the smaller dynamic range of the FTIR spectrometer and the higher noise floor of the OSA the FTIR data were scaled to match the calibrated PSD on the OSA.

To verify that the generated light was a comb in the MIR, we performed dual-comb electro-optic sampling[7] with 20 MHz resolution. Briefly, we locked the f_{ceo} of the 100 MHz oscillator using a separate f–$2f$ interferometer, while simultaneously locking one mode of the oscillator to a cavity-stabilized continuous-wave (CW) laser for repetition rate (f_{rep}) control. The CW laser linewidth of ~10 kHz was transferred to all modes. This comb system was then amplified to generate the MIR field, as described above. A second self-referenced frequency comb was generated and locked to the same CW laser, but with a slightly different repetition rate. This served as a source of <10 fs NIR pulses with which we performed electro-optic sampling of the MIR electric field with comb-tooth resolution. To verify the coherence in the UV, we measured an f_{ceo} beat using spectral overlap from the third and fourth harmonics. We observed the same free-running linewidth at 445 nm as we did at 1,000 nm using the separate f–$2f$ interferometer.

While the IP-DFG light was inherently CEP-stable with $f_{ceo}=0$ from the $\chi^{(2)}$ process, the value of f_{ceo} across the rest of the spectrum increased by exact integer values depending on the order of the nonlinear process involved. For example, the second harmonic comb had a value of $2f_{ceo}$, the third harmonic comb had a value of $3f_{ceo}$ and so on. This did not restrict the application of the comb for spectroscopy or frequency metrology, since the value of f_{ceo} was strictly harmonic and precisely known. At the same time, it would be straightforward to create the same six-octave spectrum with constant CEP by servo controlling $f_{ceo}=0$. A recent demonstration was implemented using balanced detection in the f–$2f$ interferometer[38]. This would remove any harmonics of f_{ceo} in the comb spectrum that arise from cascaded $\chi^{(2)}$ processes.

Data availability

The data supporting the findings of this study are available from D.M.B.L. upon reasonable request.

Code availability

Nonlinear Schrödinger equation code is available from citations in the Supplementary Information as well as from D.M.B.L. upon reasonable request.

References

38. Okubo, S., Onae, A., Nakamura, K., Udem, T. & Inaba, H. Offset-free optical frequency comb self-referencing with an f–2f interferometer. *Optica* **5**, 188–192 (2018).

Acknowledgements

The mention of specific companies, products or tradenames does not constitute an endorsement by the National Institute of Standards and Technology (NIST). We thank T. Schibli for his contributions and P. Schunemann and K. Zawilski at BAE for providing the CSP crystal, as well as I. Coddington, D. Carlson and M. Hummon for their manuscript feedback. D.M.B.L. and A.K. acknowledge award 70NANB18H006 from NIST. This research was supported by the Defense Advanced Research Projects Agency SCOUT Program, the Air Force Office of Scientific Research (FA9550-16-1-0016) and NIST.

Author contributions

H.T., A.K., A.J.L., D.M.B.L. and S.A.D. developed the concept. D.M.B.L., H.T., S.X., A.K. and A.J.L. built and performed the experiments. D.M.B.L. and H.T. analysed the data. D.M.B.L., H.T. and S.A.D. wrote the manuscript with input from all authors.

Competing interests

The authors declare no competing interests.

Additional information

Supplementary information The online version contains supplementary material available at https://doi.org/10.1038/s41566-021-00778-y.

Correspondence and requests for materials should be addressed to D.M.B.L. or S.A.D.

Peer review information *Nature Photonics* thanks the anonymous reviewers for their contribution to the peer review of this work.

Reprints and permissions information is available at www.nature.com/reprints.